11.2 WARM-CORE INTENSIFICATION THROUGH HORIZONTAL EDDY HEAT TRANSPORTS INTO THE EYE

Scott A. Braun
NASA, Goddard Space Flight Center
Greenbelt, Maryland

Michael T. Montgomery, John Fulton, and David S. Nolan
Department of Atmospheric Science
Colorado State University
Fort Collins, Colorado

1. Introduction

The mechanism for the formation and intensification of the hurricane warm core is not well understood. The generally accepted explanation is that the warm core forms as a result of gentle subsidence of air within the eye that warms as a result of adiabatic compression. Malkus (1958) suggested that this subsidence is part of a deep circulation in which air begins descent at high levels in the eye, acquires cyclonic angular momentum as it descends to lower levels, and then diverges at low levels, where it is entrained back into the eyewall. Inward mixing from the eyewall is hypothesized to force the subsidence and maintain the moisture and momentum budgets of the subsiding air. Willoughby (1998) suggested that air within the eye has remained so since it was first enclosed during the formation of the eyewall and that it subsides at most only a few kilometers rather than through the depth of the troposphere. He relates the subsidence to the low-level divergence and entrainment into the eyewall noted by Malkus (1958), but suggests that shrinkage of the eye's volume is more than adequate to account for the air lost to the eyewall or converted to cloudy air by turbulent mixing across the eye boundary. Smith (1980) offered an alternative view of the subsidence forcing, suggesting that vertical motion in a mature hurricane eye is generated largely by imbalances between the downward vertical pressure gradient force and the upward buoyancy force. The vertical pressure gradient force is associated with the decay and/or radial spread of the tangential wind field with height at those levels were the winds are in approximate gradient wind balance. The rate of subsidence is just that required to warm the air sufficiently such that the buoyancy remains in close hydrostatic balance with an increasing vertical pressure gradient force.

In this study, a very high-resolution simulation of Hurricane Bob (1991) using a cloud-resolving grid scale of 1.3 km is used to examine the heat budget within the storm with particular emphasis on the mechanisms for warming of the eye.

2. Numerical Model

The model used in this study is the Pennsylvania State University—National Center for Atmospheric Research nonhydrostatic mesoscale model MM5 (Dudhia 1993; Grell et al. 1995). A detailed description of the model setup is provided in Braun and Tao (2000) and Braun (2001). The analysis presented here is obtained from a 6-h simulation on a 1.3-km nest between hours 62-68 of a 72-h forecast. Model fields, including all components of the heat budget, are saved every 2 min so that the processes contributing to eye warming are well resolved in both space and time. Physics options for the 1.3-km grid include the Goddard Cumulus Ensemble Model (GCE) cloud microphysics scheme, the Burk-Thompson boundary layer parameterization, and the Dudhia (1989) cloud radiation scheme.

The storm center is determined at every model output time using the horizontal distribution of pressure at the lowest model level (42 m) to determine an approximate geometric center of the pressure field. No attempt is made to determine different centers at higher levels. Storm motion is computed from the identified near-surface center locations.

3. Results

Conventionally, heat budgets are expressed in terms of an apparent heat source Q_1 (Johnson, 1984; Houze 1982; Gallus and Johnson 1991; Braun and Houze 1996). Since our interest here is in the local warming that occurs within the eye, the heat budget is instead expressed in terms of the local tendency of potential temperature,

$$\frac{\partial \theta}{\partial t} = \text{HADV}+\text{VADV}+Q_{\text{lhr}}+Q_{\text{pbl}}+Q_r. \qquad (1)$$

HADV and VADV are the horizontal and vertical advection, respectively, Q_{lhr} the latent heating associated with cloud microphysics, Q_{pbl} the boundary layer heating, and Q_r the radiative heating. The budget is formulated in a reference frame moving with the storm so that the storm motion is included in the horizontal advection term.

Since the eye of the hurricane is dry (with the exception of the boundary layer, an upper cloud ice layer, and right along the eyewall), latent heating does not play a direct role in warming the eye. Horizontal and vertical advection and radiative heating are the main terms contributing to temperature changes within the eye. Some evaporative cooling cancels a portion of the adiabatic warming along the eyewall. In Fig. 1a, the azimuthal and time averaged sum of VADV and Q_{lhr} is used to show the net subsidence warming in the eye using contour levels that accentuate the patterns in the eye. Figure 1a clearly shows the adiabatic warming along the inner edge of the eyewall associated with moderate downdrafts there and to a lesser extent near the center. Weak adiabatic cooling occurs above 12 km

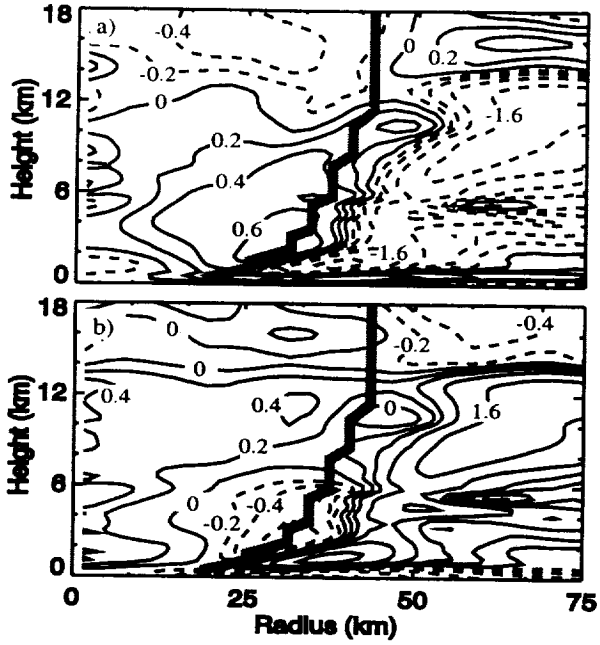

Figure 1. Azimuthal and time averaged (a) vertical advection plus latent heating and (b) horizontal advection using contours values of ±0.2, 0.4, 0.8, 1.6, 3.2, and 6.4 K h^{-1}. The irregular contour interval is used to highlight values within the eye. The thick grey line delineates the boundary between the eye and eyewall where average subsidence warming transitions to adiabatic cooling.

in the eye as a result of weak upward motion in a diffuse cloud ice layer. In the eyewall, adiabatic cooling generally exceeds latent heating except near the inner edge of the eyewall where the opposite is true. Horizontal advection (Fig. 1b) produces cooling along the inner edge of the eyewall, strongest in the region of maximum subsidence warming, and warming through much of the rest of the eye, with maximum values generally close to the center. Outside of the eye, HADV largely balances the sum of VADV and Q_{lhr} so that the net tendencies are weak. Therefore, in the eye, both VADV and HADV contribute to warming.

To determine the relative contributions from advective and radiative processes, these terms are averaged over the area of the eye, taking into account the increasing radius with height (thick, gray line in Fig. 1), and over the 6-h simulation time. The boundary of the averaging area was determined from the VADV term and marks the transition from eye warming to eyewall cooling. Figure 2a shows vertical profiles of area- and time-averaged heating rates. The profile for VADV+Q_{lhr} shows warming between 1-11 km with a peak of 0.55 K h^{-1} near 4 km. Adiabatic cooling at upper levels is generally offset by warming from longwave radiative processes in the diffuse cloud layer. Warming from HADV is concentrated in the middle to upper troposphere with a magnitude of ~0.3 K h^{-1}. Since the hydrostatic surface pressure is most sensitive to warming at upper levels (Joanne Simpson, personal communication), warming from HADV appears to play a significant role in lowering of the surface pressure. When the three terms are

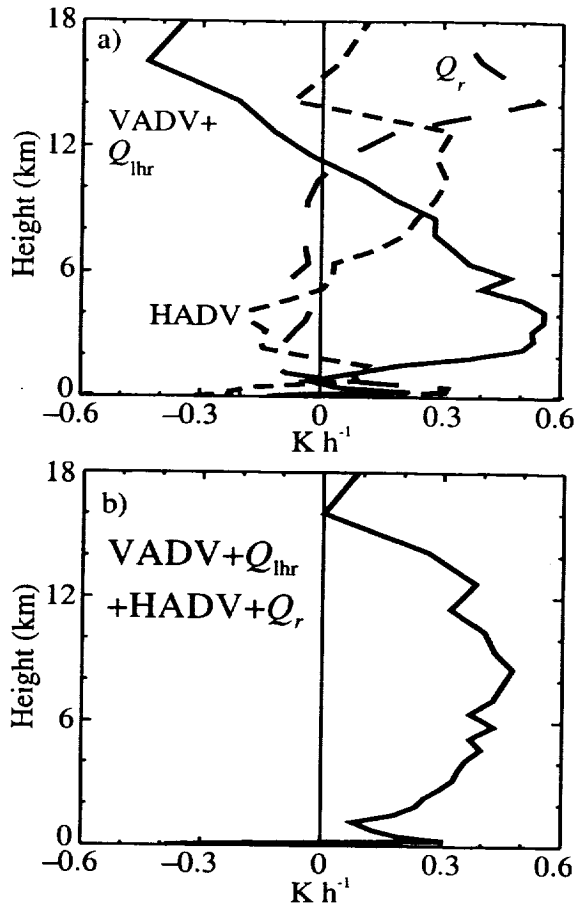

Figure 2. (a) Vertical profiles of the area and time averaged vertical advection and latent heating (solid line), horizontal advection (short-dashed line), and radiative heating (long-dashed line). (b) As in (a), but for all terms combined.

summed (Fig. 2b), the net heating profile shows average warming of 0.4-0.5 K h^{-1} peaking near 8.5 km, approximately the height of the warm anomaly (not shown). Thus, only by including the effects of horizontal advection can one account for the development of the warm core in this case.

Since the warming from horizontal advection contributes to a significant portion of the warming in the eye, it is instructive to decompose it into contributions from azimuthal mean and eddy terms as follows:

$$\overline{-u_r\frac{\partial\theta}{\partial r}-\frac{v_\lambda}{r}\frac{\partial\theta}{\partial\lambda}}=-\bar{u}_r\frac{\partial\bar{\theta}}{\partial r}-\overline{u_r'\frac{\partial\theta'}{\partial r}}-\overline{\frac{v_\lambda'}{r}\frac{\partial\theta'}{\partial\lambda}} \qquad (2)$$

where r is radius, λ azimuth, u_r and v_λ the storm-relative radial and tangential velocities, respectively, θ potential temperature, overbars indicate azimuthal averages, and the prime symbol denotes perturbations from the azimuthal mean. The azimuthal mean component of the tangential advection is zero, but the eddy component can be nonzero. The terms in (2), referred to (from left to right) as the mean horizontal advection, the mean radial advection, the eddy radial advection, and the

eddy tangential advection, are computed at each 2-min output time and averaged over the 6-h simulation period.

A radius-height cross section of the azimuthal mean horizontal advection [left side of (2)] is shown in Fig. 3a. The warming associated with the mean radial advection [first term on right in (2), Fig. 3b] accounts for the low-level cooling in the inflow and the warming within the eyewall outflow, but does not account for the cooling along the inner edge of the eyewall or the warming within the eye, which result from the eddy components. The radial eddy advection (Figs. 3c) produces the bulk of the cooling along the inner edge of the eyewall and about half of the warming in the eye. The tangential eddy advection (Figs. 3d) produces warming in the eye through most of the troposphere, while along the inner edge of the eyewall, it produces upper level warming and weak low-level cooling. Within and outside of the eyewall, the radial eddy component is much stronger than the tangential eddy component.

These eddy components can be further decomposed into contributions from different azimuthal wavenumbers (not shown). The main contributions to the warming in the eye come from the wavenumber 1 components of both the radial and tangential eddy terms. Although wavenumber 2 asymmetries play a significant role in the structure and evolution of the eyewall (Braun 2001), their contributions to eye warming are generally small. The impacts of wavenumbers 3 and higher are strong, but are confined to the region close to the eyewall.

Figure 4 shows the wavenumber 1 potential temperature anomalies and wind vectors at 10.4 km, which are representative of the layer between 5-11 km. The potential temperatures are generally warmer on the western side of the storm, cooler on the eastern side, with the maximum anomalies in the eyewall. The orientation of the peak temperature anomalies in the eyewall are rotated somewhat counterclockwise relative to the anomalies just outside the eyewall and within the eye. Approximately collocated with the peak temperature anomalies are counter-rotating vortices with the warm (cold) anomaly associated with an anticyclonic (cyclonic) vortex. Airflow outside of the eyewall is directed toward the northwest, approximately in the direction of the mean environmental storm-relative flow. Inside the eye, the flow moves in the opposite direction between the two vortices. This flow pattern is nearly identical to that observed at mid-to-upper levels in Hurricane Norbert [1984, Marks et al. (1992)]. Marks et al. (1992) argued that these small-scale gyres were similar to gyres associated with a linear barotropic instability of the mean vortex as described by Peng and Williams (1990). The study of Nolan and Montgomery (2000) suggests that this flow field is related to a steady wavenumber 1 neutral mode, or pseudomode, that represents a linear displacement of the vortex. A growing normal mode and vortex Rossby waves may also play important roles and will be investigated in the future. These studies suggest that the gyres may be characteristic features of mature hurricanes. The airflow within the eye is oriented roughly 45° with respect to the orientation of the warm anomalies such that the flow transports warmer air in and cooler air out of the eye.

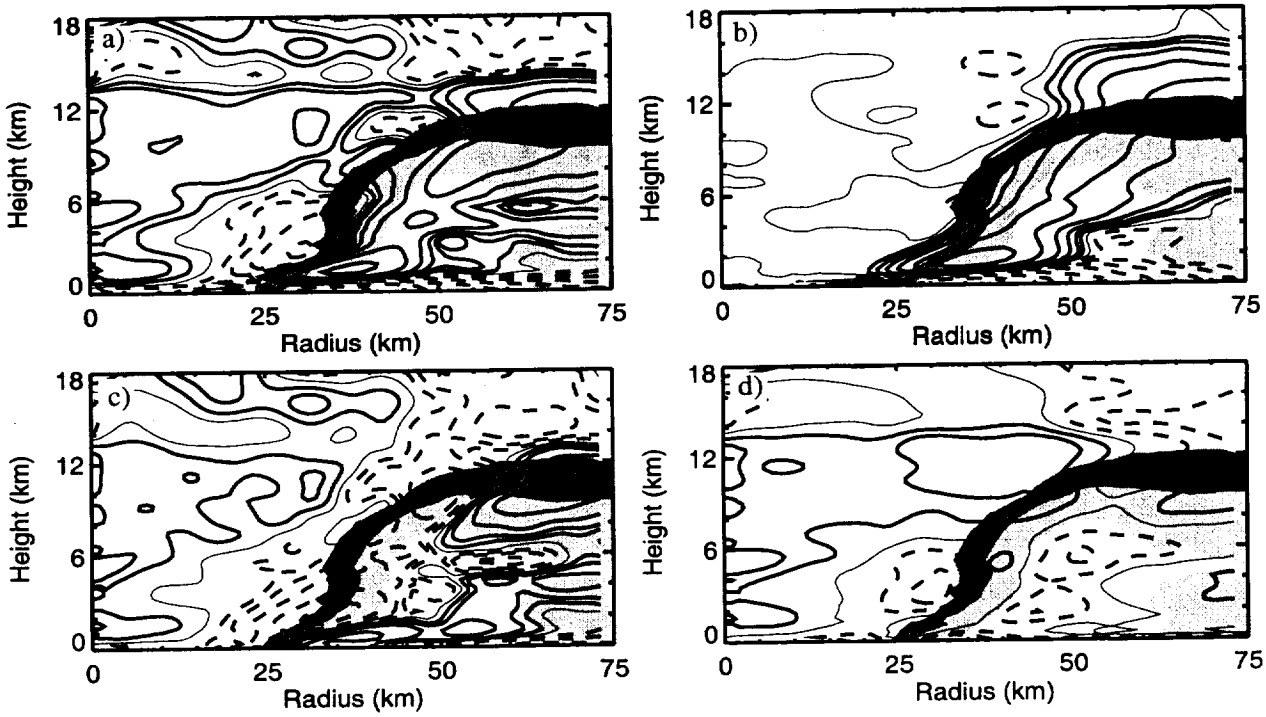

Figure 3. Azimuthal and time averaged cross sections of (a) total horizontal advection, (b) mean radial advection, (c) eddy radial advection, and (d) eddy tangential advection. Shading indicates simulated radar reflectivity at values of 5, 20, and 35 dBZ. Contours for advection fields are drawn at ±0, 0.1, 0.2, 0.4, 0.8, 1.6, 3.2, 6.4 K h^{-1}. Positive (negative) values are indicated by solid (dashed) lines. The thin contour indicates values of zero.

5. Conclusions

The calculations indicate an important role of horizontal eddy heat transports into the eye and suggest a new conceptualization of the process by which the warm core of the eye intensifies. This warming by horizontal advection is counter to heat exchange by mixing across the mean vortex since the mean eyewall air is typically cooler than that of the eye. The warming of the eye by horizontal eddy heat transports is consistent with idealized model calculations of asymmetric disturbances that form on three-dimensional, baroclinic vortices (Moller and Montgomery 2000; Nolan and Montgomery 2000). These vortex Rossby waves import not only momentum (Montgomery and Kallenbach, 1997) but also heat into the eye (Montgomery and Enagonio, 1998).

The warming from horizontal advection has been shown to be the result of azimuthal eddies, which means that asymmetries in the eyewall structure are contributing to warming of the eye. The mechanism by which these asymmetries warm the eye needs to be explored further. Since tropical cyclones often undergo transitions from asymmetric systems to more symmetric systems, it is important to develop an understanding of how this process varies during transition. Such understanding can provide the critical linkage between these eddies and convective blowups in the eyewall (observable from satellite and aircraft remote sensing) and their relationship with rapid intensification, which may then lead to improved forecasts of intensity change.

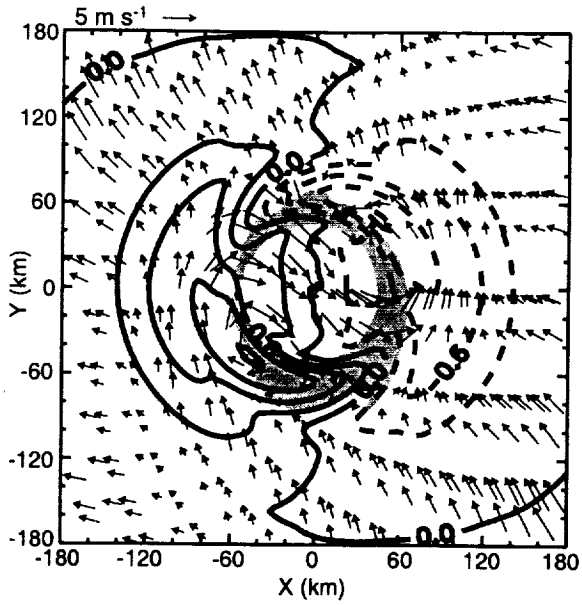

Figure 4. Time-averaged wavenumber 1 potential temperature (contours) and wind anomalies (vectors) at 10.4 km MSL. Contours are drawn at intervals of 0.3 K. Shading denotes time-averaged vertical motions in excess of 1 m s^{-1}.

REFERENCES

Braun, S. A., and R. A. Houze, Jr., 1996: The heat budget of a midlatitude squall line and implications for potential vorticity production. *J. Atmos. Sci.*, **53**, 1217-1240.

Braun, S. A., and W.-K. Tao, 2000: Sensitivity of high-resolution simulations of Hurricane Bob (1991) to planetary boundary layer parameterizations. *Mon. Wea. Rev.*, **128**, 3941-3961.

Braun, S. A., 2001: A cloud-resolving simulation of Hurricane Bob (1991): Storm structure and eyewall buoyancy. *Mon. Wea. Rev.*, (submitted).

Dudhia, J., 1993: A nonhydrostatic version of the Penn State-NCAR mesoscale model: Validation tests and simulation of an Atlantic Cyclone and cold front. *Mon. Wea. Rev.*, 121, 1493-1513.

Dudhia, J., 1989: Numerical study of convection observed during the Winter Monsoon Experiment using a mesoscale two-dimensional model. *J. Atmos. Sci.*, 46, 3077-3107.

Gallus, W. A., Jr., and R. H. Johnson, 1991: Heat and moisture budgets of an intense midlatitude squall line. *J. Atmos. Sci.*, **48**, 122-146.

Grell, G. A., J. Dudhia, and D. R. Stauffer, 1995: A description of the fifth-generation Penn State/NCAR Mesoscale Model (MM5). NCAR Technical Note (NCAR/TN-398+STR), 122 pp.

Houze, R. A., Jr., 1982: Cloud clusters and large-scale vertical motions in the Tropics. *J. Meteor. Soc. Japan*, **60**, 396-410.

Johnson, R. H., 1984: Partitioning tropical heat and moisture budgets into cumulus and mesoscale components: Implications for cumulus parameterization. *Mon. Wea. Rev.*, **112**, 1590-1601.

Malkus, J. S., 1958: On the structure and maintenance of the mature hurricane eye. *J. Meteor.*, **15**, 337-349.

Marks, F. D., R. A. Houze, Jr., and J. F. Gamache, 1992: Dual-aircraft investigation of the inner core of Hurricane Norbert. Part I: Kinematic structure. *J. Atmos. Sci.*, **49**, 919-942.

Moller, J. D., and M. T. Montgomery, 2000: Tropical cyclone evolution via potential vorticity anomalies in a three-dimensional balance model. *J. Atmos. Sci.*, **57**, 3366-3387.

Montgomery, M. T., and R. J. Kalenbach, 1997: A theory for vortex Rossby waves and its application to spiral bands and intensity changes in hurricanes. *Quart. J. Roy. Meteor. Soc.*, **123**, 435-465.

Montgomery, M. T., and J. Enagonio, 1998: Tropical cyclogenesis via convectively forced vortex Rossby waves in a three-dimensional quasigeostropic model. *J. Atmos. Sci.*, **55**, 3176-3207.

Nolan, D. S., and M. T. Montgomery, 2000: The algebraic growth of wavenumber one disturbances in hurricane-like vortices. *J. Atmos. Sci.*, **57**, 3514-3538.

Peng, M. S., and R. T. Williams, 1990: Dynamics of vortex asymmetries and their influence on vortex motion on a β-plane. *J. Atmos. Sci.*, **47**, 1987-2003.

Smith, R. K., 1980: Tropical cyclone eye dynamics. *J. Atmos. Sci.*, **37**, 1227-1232.

Willoughby, H. E., 1998: Tropical cyclone eye thermodynamics. *Mon. Wea. Rev.*, **126**, 3053-3067.